ARMY RESEARCH LABORATORY

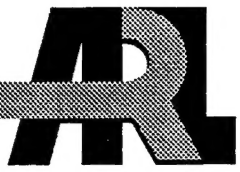

Modeling the Effect of Penetrator Nose Shape on Threshold Velocity for Thick Aluminum Targets

by Daniel R. Scheffler

ARL-TR-1417 July 1997

The findings in this report are not to be construed as an official Department of the Army position unless so designated by other authorized documents.

Citation of manufacturer's or trade names does not constitute an official endorsement or approval of the use thereof.

Destroy this report when it is no longer needed. Do not return it to the originator.

Army Research Laboratory
Aberdeen Proving Ground, MD 21005-5066

ARL-TR-1417 **July 1997**

Modeling the Effect of Penetrator Nose Shape on Threshold Velocity for Thick Aluminum Targets

Daniel R. Scheffler
Weapons and Materials Research Directorate, ARL

Abstract

This study examines the ability of the CTH hydrocode to predict the effects of rod nose shape on the threshold impact velocity, whereby tungsten alloy long rods transition from rigid-body to eroding-rod penetration during penetration or perforation of thick aluminum targets. Two rod nose shapes (hemispherical and ogival) were used in the simulations, and two aluminum alloys (5083 and 7039) were used as the target materials. The predicted results are compared to an experimental study. Predictions of the threshold velocity for the ogival-nose rod are offered.

Acknowledgments

The author would like to thank Mr. Kent D. Kimsey and Mr. Todd W. Bjerke for their helpful comments and suggestions regarding this report. The author would especially like to thank Dr. Lee S. Magness, Jr. for his helpful advice regarding the direction of research taken, his willingness to discuss and share his work, and assurance regarding the accuracy of the discussion of his experiments. An additional thanks goes to Dr. Stewart A. Silling of Sandia National Laboratories for discussions regarding his boundary layer interface algorithm and for providing an advance copy of parts of his user manual.

INTENTIONALLY LEFT BLANK.

Table of Contents

INTENTIONALLY LEFT BLANK

List of Figures

List of Tables

INTENTIONALLY LEFT BLANK.

1. Introduction

In examining the convergence characteristics of the Eulerian CTH hydrocode [1] as a function of spacial resolution, Zukas [2] found that the code could not accurately predict perforation of armor plate by a hard projectile at low velocities (less than 1.5 km/s). A penetrator, which, in experiments, perforated a finite steel target with significant residual length and velocity, was predicted to be unable to perforate the target. Previously, this problem had been modeled successfully using an in-house version of the EPIC Lagrangian hydrocode. Zukas observed that, regardless of the mixed cell strength formulation used (several are available in CTH), high-strength penetrator material included in a mixed cell was modeled as being significantly softer, an unrealistic treatment that caused excessive deformation in the penetrator. The net effect was that the CTH hydrocode could not accurately model the rigid-body penetration of a soft target, an eroding projectile penetrating harder targets at low velocities or sliding between two material interfaces.

A new boundary layer algorithm for sliding interfaces (BLINT) was recently incorporated into the CTH hydrocode for two-dimensional problems only [3]. The algorithm relocates the slip layer outside of the mixed cells and into the softer material, thus allowing hard materials to penetrate as rigid bodies. Good correlation with experiments have been obtained using the BLINT algorithm by Silling [4] and Kmetyk and Yarrington [5]. They modeled hard penetrators impacting soft targets knowing a priori that the penetrators would remain rigid.

This study examined the ability of the CTH hydrocode (August 1993 release) to predict the impact velocity at which a penetrator would transition from rigid-body to eroding-rod penetration and the effect of a penetrator's nose shape on this transition velocity. The perforation of soft aluminum targets by tungsten alloy (95W-2.5Ni-1.0Fe-1.5Co, cold-worked by swaging to a 21% reduction in area) long rods was modeled. To gauge the accuracy of the CTH hydrocode with the BLINT algorithm, the simulation results were compared to the experimental depth of penetration (DOP) tests [6]. Two rod nose shapes and two target alloys were considered. The rod nose shapes

were hemispherical and ogival, and the target alloys were 53.34-cm-thick 5083 aluminum and 7039 aluminum.

The results of this study first appeared in at the Fourth International Conference on Structures Under Shock and Impact (SUSI96) that took place in Udine, Italy from July 3 to 5, 1996 [7]. At that time the experiments involving the ogival-nose penetrator were not complete; therefore, predictions for the ogival-nose penetrators were offered in advance of the experiments. While it now appears that the semi-infinite penetration experiments involving the ogival-nose penetrator will not be completed, due to lack of funding, experiments for finite 7039 aluminum targets have been completed. The predicted threshold velocity for the finite 7039 aluminum target is included herein to compare with the CTH hydrocode predictions. This report differs from the original paper by including the additional experimental results for comparison with a more detailed description of the BLINT model and by providing the input decks used for the simulations.

The CTH hydrocode is a state-of-the-art, second-order accurate, Eulerian wave propagation code developed by Sandia National Laboratories that is capable of solving complex problems in shock physics in one, two, or three dimensions. The code provides several constitutive models, including an elastic perfectly plastic model with provisions for work-hardening and thermal-softening, the Johnson-Cook model [8], the Zerilli-Armstrong model [9], the Steinberg-Guinan-Lund model [10, 11], and an undocumented power-law model. High explosive detonation can be modeled using a programmed burn model, the Chapman-Jouguet volume burn model, or the history variable reactive burn model [12]. Several equation-of-state (EOS) options are available, including tabular (i.e., SESAME), analytical (ANEOS), Mie-Gruneisen, and Jones-Wilkins-Lee (JWL) [13]. Material failure occurs when a threshold value of tensile stress or hydrostatic pressure is exceeded. In addition, the Johnson-Cook failure model [14] is also available. When failure occurs in a cell, void is introduced until the stress state of the cell is reduced to zero. Recompression is permitted. To reduce material diffusion typically encountered in Eulerian simulations, several advanced material interface tracking algorithms are provided including the high-resolution interface tracking (HRIT) algorithm (available for two-dimensional simulations only), the simple line interface calculation (SLIC) algorithm [15], and the Sandia-modified Youngs' reconstruction algorithm (SMYRA) [16].

2. Problem Setup

The two geometries for the tungsten alloy penetrators are shown in Figure 1. The ogival-nose penetrator has a length of 10.1346 cm and a diameter of 0.67568 cm. The length of the hemi-nose penetrator was shortened to 9.779 cm, such that both penetrators had the same nominal mass of 63 g.

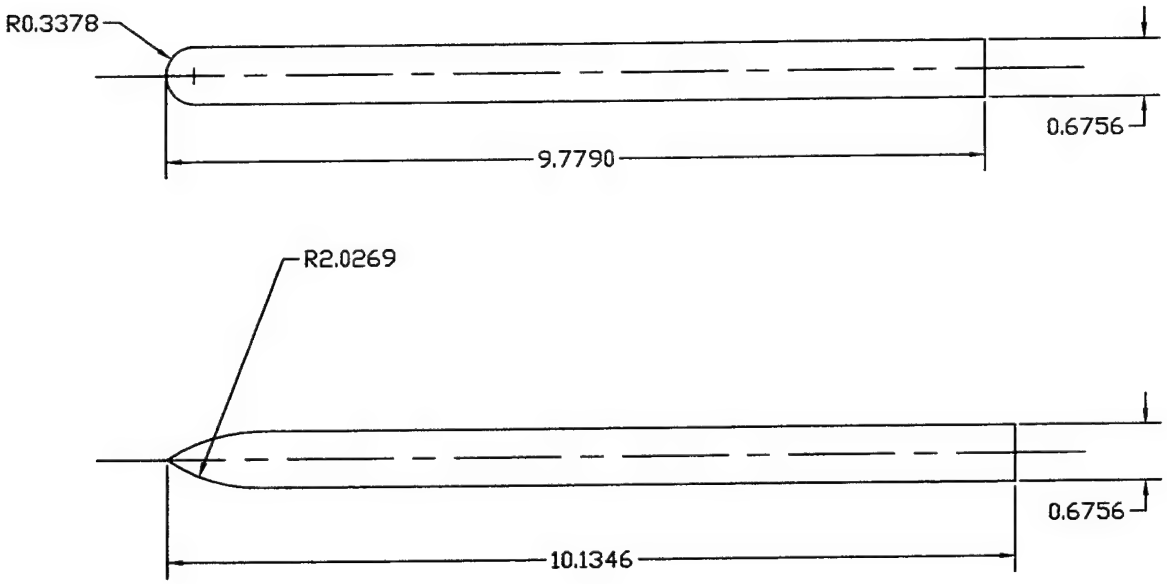

Figure 1. Penetrator Geometries.

Three different constitutive models were used in the simulations to model the deviatoric response of the materials. The choice of the constitutive model used for a material was governed by the availability of material data. Material data were not available for the 95W-2.5Ni-1.0Fe-1.5Co, 21% swaged tungsten alloy penetrators used in the experiments. Therefore, the alloy was approximated using 95W-3.5Ni-1.5Fe tungsten alloy data for the Steinberg-Guinan-Lund strain-rate-independent model reported in Steinberg [17]. This tungsten alloy has the same percentage of tungsten and the same approximate density as the 95W-2.5Ni-1.0Fe-1.5Co, 21% swaged alloy. For the 7039 aluminum target, the Johnson-Cook constitutive model was used with parameters reported in

Johnson and Cook [8]. For the 5083 aluminum target, a power-law constitutive model was used with parameters reported in Silling [3] and originally reported in Forrestal, Luk, and Brar [18].

The Mie-Gruneisen EOS was used for all materials. EOS data were obtained from a data file provided with the CTH hydrocode. The EOS parameters for 5083 aluminum, 7039 aluminum, and 95% tungsten content tungsten alloy were not available. Therefore, they were approximated using parameters for 6061 aluminum, 7075 aluminum, and 90W-7Ni-3Fe tungsten alloy, respectively. The initial density of the 6061 and the 7075 aluminum alloys were changed to reflect values for 5083 and 7039 aluminum, as reported in the Metals Handbook Desk Edition [19]. The initial density of the 90W-7Ni-3Fe alloy was changed to reflect the initial density of the 95W-3.5Ni-1.5Fe alloy reported in Steinberg [17]. The EOS parameters used for all materials are listed in Table 1.

Table 1. EOS Parameters

Material	Density ρ_o (g/cm^3)	Sound Speed c_o (km/s)	U_s–U_p Slope	Gruneisen Parameter Γ_o	Specific Heat c_v (erg/g/eV)
W Alloy	18.16	4.03	1.237	1.67	1.66e11
5083 A1	2.66	5.34	1.40	1.97	1.07e11
7039 A1	2.77	5.20	1.36	2.20	1.07e11

Failure in most of the simulations was modeled using a threshold tensile pressure criterion. The tensile pressure at which the tungsten alloy, the 5083 aluminum, and the 7039 aluminum were assumed to fail was 3.5 GPa, 0.45 GPa, and 0.50 GPa, respectively. Additional simulations used a strain-based failure criterion that is described later in this report.

All simulations used a two-dimensional cylindrical coordinate mesh consisting of 85 × 1545 cells. The mesh in the radial direction starts at the axis of symmetry with a constant cell size of 0.0422275 cm out to a radius of 1.6891 cm. Thereafter, cell dimensions expand by 5% increments out to the outer radius of the target. This mesh provides eight cells across the radius of the

penetrator. The mesh in the axial direction has a constant cell size of 0.0422275 cm. Thus, cells in the penetrator-target interaction region have a uniform one-to-one aspect ratio.

Parameters for the BLINT model were chosen to be similar to those reported in Kmetyk and Yarrington [5]. Thus, the boundary-layer distance (w_{bl}) and the slip-layer distance (w_{sl}) were chosen to be twice the zone size of cells in the penetrator-target interaction region. The boundary-layer distance defines which cells will be included in the boundary layer. If the cell center of a cell is located w_{bl} away from a cell whose center is included in the interface layer, it is considered to be part of the boundary layer. The interface layer, which is about two cell widths thick, contains all cells whose hard and soft volume fraction vector gradiant magnitudes are both greater than or equal to 0.1. The slip-layer distance defines which cells will be included in the slip layer. If the cell center of a cell located in the soft boundary layer is w_{sl} from a cell whose center is included in the interface layer, it is consider part of the slip layer. Cells located in the slip layer have their flow stresses set to zero, allowing sliding to occur in these cells. An option to automatically increase the yield strength of the penetrator material by a factor equal to

$$\left(\frac{r_o + w_{bl}}{r_o} \right)^2$$

(where r_o is the outer radius of the penetrator) was used. This option was used because numerical noise can cause shear stresses close to the yield stress to exceed the yield stress, causing premature irreversible deformation of the penetrator. An additional option allows for the inclusion of friction. However, friction between the target and penetrator was not modeled in this study. Kmetyk and Yarrington [5] showed that the BLINT model tended to overpredict penetration in deep penetration problems unless friction was included.

The CTH hydrocode cannot convect velocity in a manner such that both momentum and kinetic energy (KE) are both conserved exactly. The default option allows conservation of KE such that total energy is conserved during the convection phase of a computational cycle; however, momentum is not conserved. A second option convects velocity such that momentum is conserved during the convection phase of a computational cycle, and any KE discrepancies are discarded (this is the only

available option in newer releases of CTH). Simulations were run using both convection options. Simulations that conserved KE during the convection phase of a computational cycle will be referred to as KE Sim(s), and those conserving momentum during the convection phase of a computational cycle will be referred to as MV Sim(s). A final option conserves both momentum and total energy during the convection phase of a computational cycle by depositing the KE discrepancy into internal energy. This can have the effect of artificially heating a material; therefore, this option was not used.

A complete listing of the CTH input data decks used for the simulations is given in Appendices A–E. If the only differences between input decks was the striking velocity, conservation method, or whether or not the BLINT model is used, then those input decks are not listed. Notes in the input decks describe the required changes needed for the input decks not listed.

3. Results and Discussion

Initial impact conditions and ballistic test results [6] used for comparison are provided in Table 2. The penetration depths listed were measured perpendicular to the original target surface along the penetrator's original flight line. In some cases, the penetration channel was significantly curved; therefore, the total path length traveled by the penetrator may have been greater than the listed penetration depth. The total yaw values for the penetrators were quite small (in most cases less than 1°). However, these yaw values still exceed the critical yaw as defined in Bjerke et al. [20, 21], since the penetration channel diameter is about the same as the penetrator shank diameter for rigid-body penetration of soft targets (e.g., see Forrestal et al. [22]). Any effects of yaw were not treated in these two-dimensional simulations.

The increase in penetration depth for rigid-body, long-rod penetrators penetrating soft targets is nearly directly proportional to the striking velocity, except at extremely low striking velocities (less than 600 m/s). However, as impact velocity is increased further, the stresses in the nose of the penetrator will eventually exceed the yield strength of the penetrator material. The penetrator will

Table 2. Initial Impact Conditions and Ballistic Test Results

Shot No.	Total Yaw (°)	Striking Velocity (m/s)	Original Mass (g)	Penetration (cm)
Hemi-Nose Penetrator vs. 7039 Aluminum Target				
4338	0.50	1,165	62.7	11.4 est.
4339	0.25	1,038	63.1	28.3
4340	0.50	1,248	63.1	13.0
Ogival-Nose Penetrator vs. 7039 Aluminum Target				
4341	0.90	1,156	63.4	37.7
4342	0.56	1,291	63.4	>53.3
4343	0.71	1,075	63.1	35.4
Hemi-Nose Penetrator vs. 5083 Aluminum Target				
4344	0.50	1,086	62.8	44.8
4345	0.35	1,200	63.0	20.0
4346	0.25	1,296	62.9	21.6
Ogival-Nose Penetrator vs. 5083 Aluminum Target				
4347	0.50	923	62.9	41.7
4348	1.12	1,070	63.1	39.9
4349	0.80	1,227	62.8	>53.3

begin to deform plastically, and the increase in penetration with increasing striking velocity ceases to be nearly linear. The deformation and erosion of the penetrator at these higher velocities leads to a dramatic drop in the penetration depth. Still, further increases in striking velocity will again result in a second region displaying a near-linear increase in penetration depth with increasing striking velocity. The plot of penetration depth as a function of impact velocity will eventually level off as the penetrator approaches the hydrodynamic limit given by

$$L_0\left(\frac{\rho_p}{\rho_t}\right)^{\frac{1}{2}}$$

where L_0 is the initial rod length, and ρ_p and ρ_t are the penetrator and target densities, respectively.

Experimental DOP results, as well as the predictions from the KE Sims and the MV Sims for the 5083 and 7039 aluminum targets are shown in Figure 2(a) and (b), respectively. The experimental results are represented with solid symbols, the KE Sims are represented with hollow symbols, and the MV Sims are represented with half-filled symbols. In addition, the hemi-nose penetrators are represented by circles, the ogival-nose penetrators are represented by squares, and the rear of the target is represented with a dotted line. If a penetrator perforated the target, it is represented by an error bar on the symbol. Examining only the predictions of the hemi-nose penetrators in Figure 2(a) and (b), it is apparent that both the KE Sims and the MV Sims show the same trends observed experimentally. The KE Sims more accurately predicted the transition velocity from rigid-body to eroding-rod penetration (reflected by the decrease in penetration depth). The MV Sims predicted that the transition would occur at approximately a 100-m/s higher impact velocity than the experiment and appear to consistently overpredict the final DOP at most velocities. This may be due, in part, to the KE Sims more accurately predicting the projectile shape than the MV Sims (e.g., see Scheffler [23]). For this reason, it was decided to predict the threshold velocity at which the ogival-nose penetrators transition from rigid rod to eroding penetrator, using only the KE Sims. The CTH hydrocode simulations predicted that the transition velocity for the ogival-nose penetrator would lie between 1,900 and 2,000 m/s for the 5083 aluminum targets and between 1,800 and 1,900 m/s for the 7039 aluminum targets. Ballistic experiments of the ogival-nose penetrator will no longer be attempted to confirm these predictions, due to lack of funding. Limited test data against thinner targets [6] has confirmed that the transition velocity for the ogival-nose penetrator lie above 1,700 m/s for both aluminum alloys. Ballistic tests against 7.62-cm-thick 7039 aluminum targets have shown the transition velocity for the ogival-nose penetrator to lie between 1,755 and 1,768 m/s [6]. This compares favorably with the CTH-predicted transition velocity between 1,800 and 1,900 m/s.

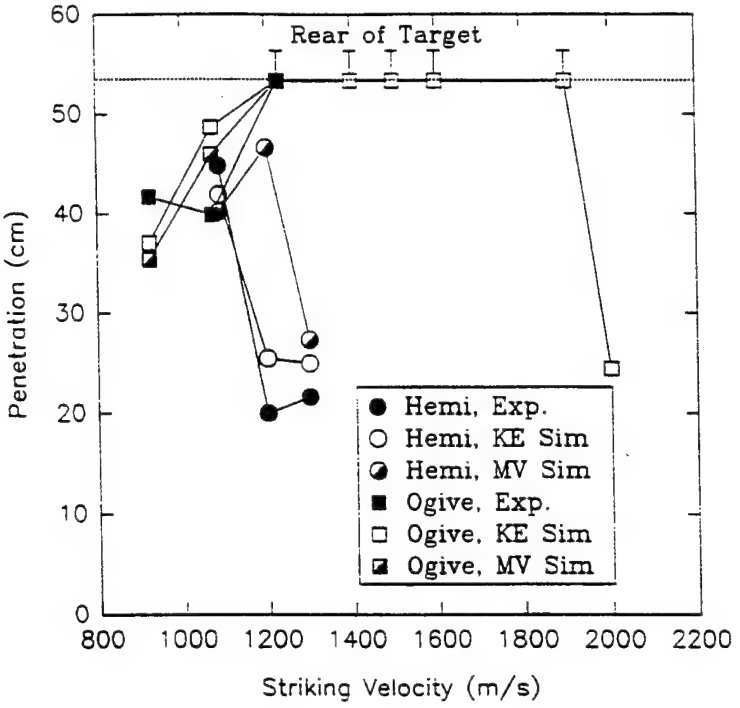

(a) 5083 Aluminum Targets.

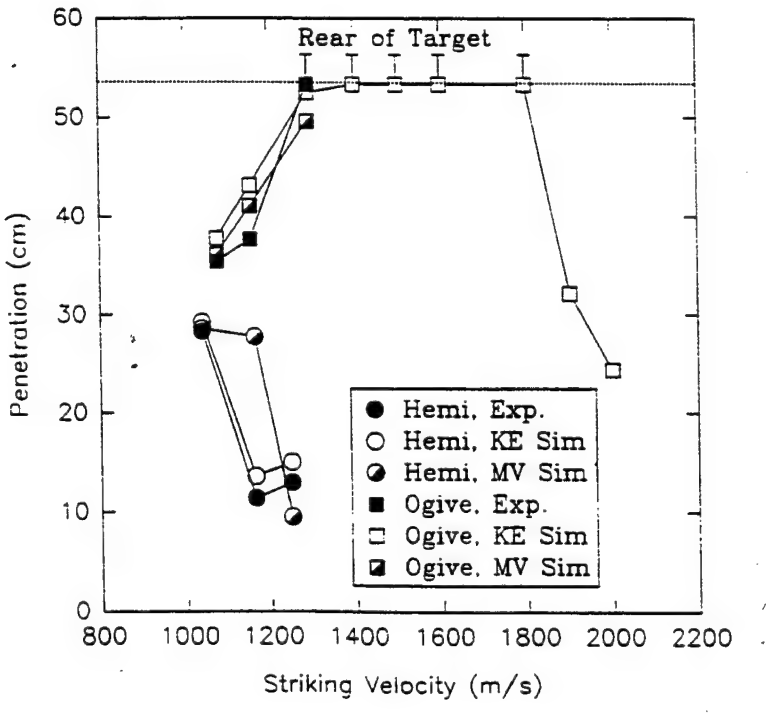

(b) 7039 Aluminum Targets.

Figure 2. Comparison of KE Sims and MV Sims with Experiment.

While the CTH hydrocode seems to have done an adequate job of predicting the threshold velocity at which hemi-nose penetrators transition from rigid body to eroding rods, it tended to overpredict the actual penetration values. This may have been due, in part, to the exclusion of friction in the simulations. The BLINT model was added to the CTH hydrocode in order to model rigid-body penetration. Therefore, once the transition to eroding-rod penetration occurs, the model may no longer be necessary or accurate. For this reason, the KE Sims for which the BLINT model seemed to predict erosion were repeated with the BLINT model turned off. Results of these simulations are shown in Figure 3(a) and (b) for the 5083 and 7039 aluminum targets, respectively. The symbols in Figure 3 are the same as those in Figure 2, with the exception that half-filled symbols represent simulations where the BLINT model was turned off. In examining the figures, it is apparent that all of the simulations with the BLINT turned off underpredict the experiment. This may, in part, be due to the fact that the option in the BLINT model to increase the penetrator's yield strength was no longer in use and, in part, due to the mixed cell treatment artificially reducing the strength of penetrator material in mixed cells. The difference between prediction and experiment is less for the ogival-nose rods because the influence of material strength is less at higher impact velocities.

While the results so far suggest that the BLINT model appears to predict, at least for the hemi-nose KE Sims, the velocity of transition from rigid body to eroding rod, it does not show the penetrators eroding in their typical mushroom-head fashion. Instead, the penetrators simply deformed with little, if any, noticeable erosion occurring. Magness [24] suggested that the threshold tensile pressure failure model used might be the cause. Reasons for this are given in the paper by Magness [25] discussing the properties of KE penetrators. To investigate the effect of the failure model, all simulations for the hemi-nose penetrator impacting 5083 aluminum at a striking velocity of 1,296 m/s were repeated using the Johnson-Cook failure model with all but the first parameter turned off. All material would now be set to fail at a strain of 150%. Final projectile shapes are shown in Figure 4. Only the projectile material is shown in Figure 4 in order to show the erosion products. The projectiles are designated XX-XX-X, where the first two X's represent KE Sim (KE) or MV Sim (MV), the second set of X's represents BLINT model (BL) or no-BLINT model (NB), and the final X represents threshold tensile pressure failure model (P) or threshold strain model

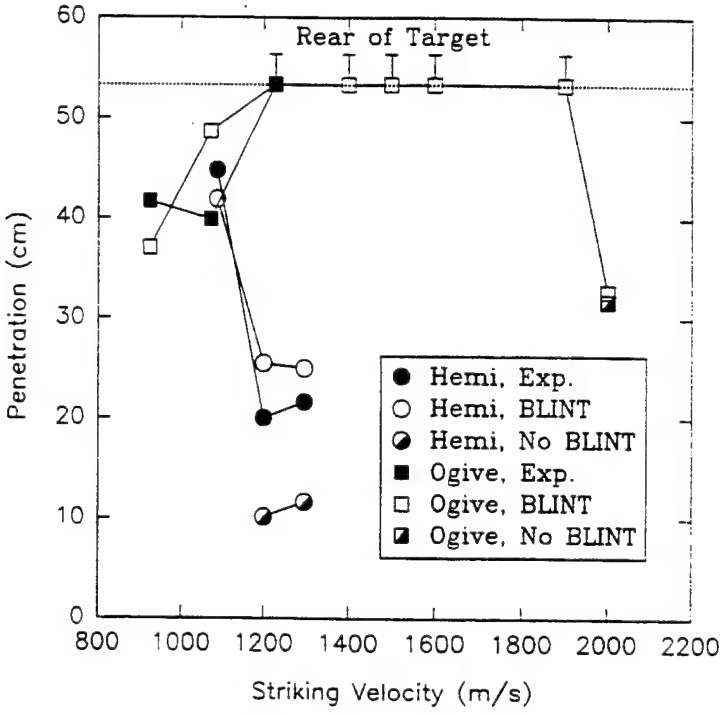

(a) 5083 Aluminum Targets.

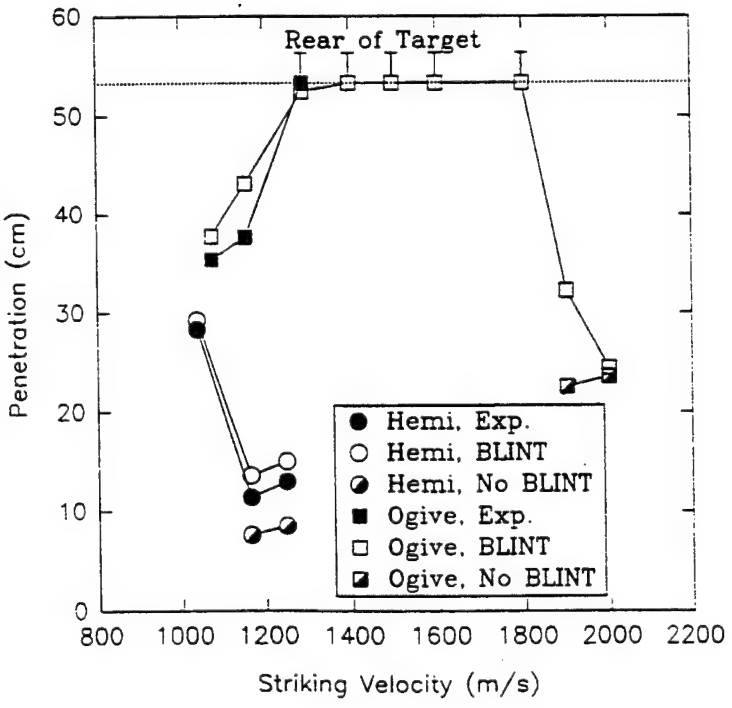

(b) 7039 Aluminum Targets.

Figure 3. Comparison of KE Sims With and Without BLINT Model With Experiment.

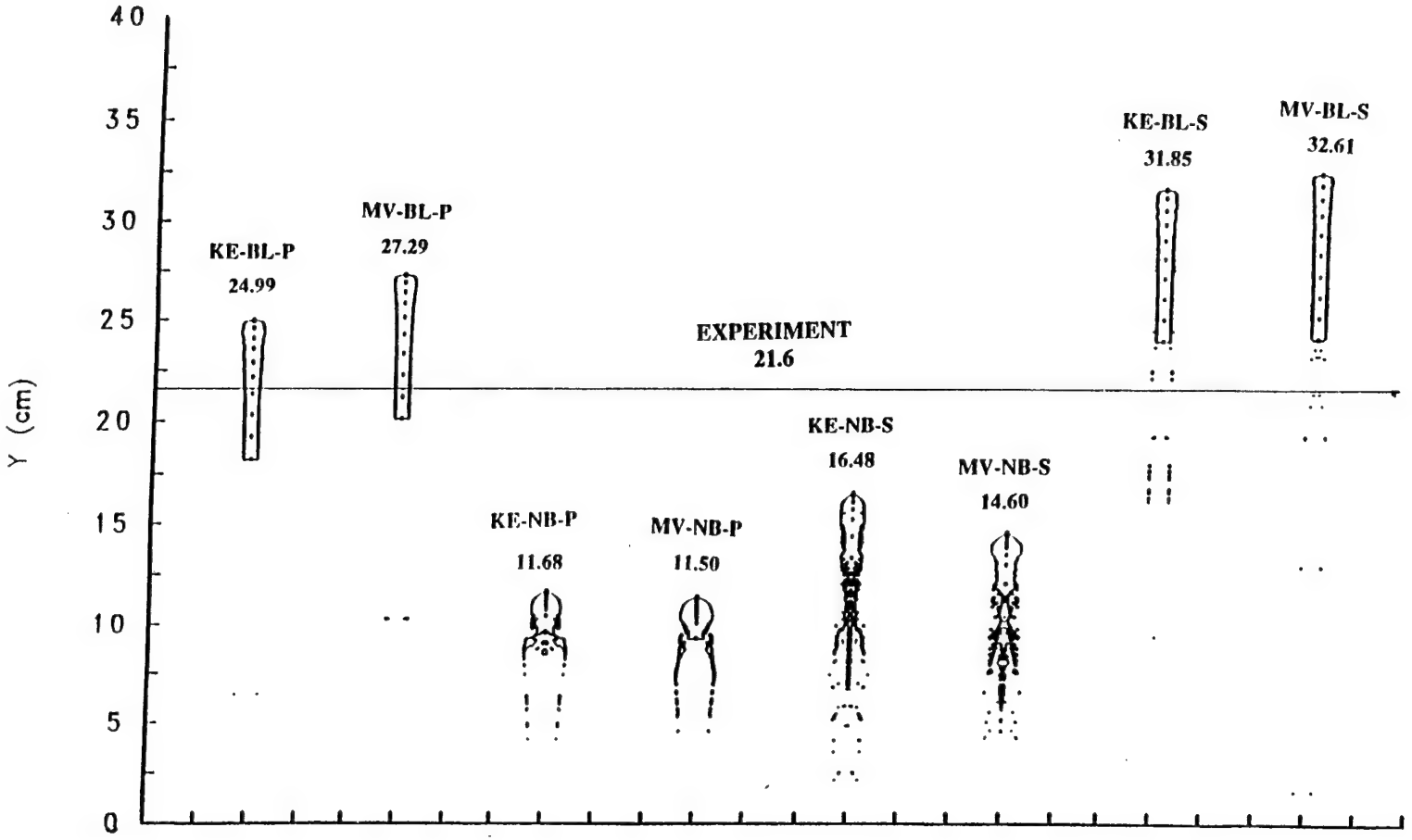

Figure 4. Comparison of Hemi-Nose Penetrator Simulations With a Striking Velocity of 1,296 m/s Impacting a 5083 Aluminum Target.

using Johnson-Cook failure (S). Thus, a designation of KE-BL-P means the simulation was a KE Sim with the BLINT model turn on and used the threshold tensile pressure failure model. Under the projectile designation is the predicted penetration depth in centimeters. Experimentally, the penetration was 21.6 cm and is represented with a horizontal line in Figure 4. The vertical axis in Figure 4 represents the penetration depth.

From Figure 4, it is apparent that very little erosion took place in the KE-BL-P and MV-BL-P simulations (KE Sim and MV Sim from Figure 2), and that the drastic drop in penetration seen in Figure 2 was due to plastic deformation. Turning the BLINT model off caused a more typical erosion event to occur, but also caused excessive deformation in the penetrator (KE-NB-P and MV-NB-P simulations). Keeping the BLINT model turned off and changing to a strain-based failure model increased the predicted penetration values, and the deformation of the penetrator more closely resembled those observed by Magness [25]. With the BLINT model turned on in conjunction with a strain-based failure model, the simulations show that some erosion occurs, but not as much as expected and the final DOP was over predicted (KE-BL-S and MV-BL-S simulations). In all cases, the KE Sims predictions were closer to the experimental result than were their MV Sims counterparts.

4. Conclusions

It is known that the constitutive response of tungsten alloy is dependent on strain, strain rate, tungsten content, grain size, and amount of swaging [26]. In addition, for solid-solid impacts at velocities of 500 to 2,000 m/s, initial impact pressures rapidly decay to values comparable to the strength of the material. Therefore, the constitutive model is of primary importance in this impact regime, and the EOS is of secondary importance [27]. It is probably unrealistic to expect the simulation results with the constitutive model approximations and simple failure models used to provide an exact match with the experimental data. Nevertheless, the following conclusions are offered.

The BLINT model represents an improvement in the predictive capabilities of the CTH hydrocode for certain types of penetration scenarios, such as rigid-body penetrations. The code seems to be able to predict the effect on rod nose shape on the threshold velocity at which transition from rigid-body to eroding-rod penetration occurs. The predicted transition velocity was determined from a dramatic drop in penetration depth with increasing impact velocity. Predictions for the transition velocity from rigid-body to eroding-body penetration were offered in advance of experiments for the ogival-nose penetrators. The simulations predict the transition velocity to be between 1,900 and 2,000 m/s for the 5083 aluminum targets and between 1,800 and 1,900 m/s for the 7039 aluminum targets. While the experiments for the ogival-nose penetrator will probably not be completed, due to lack of funding, completion of experiments for the ogival-nose penetrator against a thinner 7039 aluminum target shows the transition velocity to be between 1,755 and 1,768 m/s. Thus, the predicted transition velocity between 1,800 and 1,900 m/s compares favorably with Magness' ballistic test data [6].

In general, the KE Sims did much better than the MV Sims at predicting the transition velocity at which hemi-nose penetrators transition from rigid-body to eroding-rod penetration, as well as at predicting the DOP. The KE Sims also did better than their MV Sims counterparts in predicting the DOP in the study comparing failure models and in the study comparing simulations with and without the BLINT model.

5. References

1. Mc Glaun, J. M., S. L. Thompson, M. G. Elrick. "CTH: A Three-Dimensional Shock Wave Physics Code." *International Journal of Impact Engineering*, vol. 10, nos. 1–4, pp. 251–360, 1990.

2. Zukas, J. A. U.S. Army Research Laboratory Memorandum, Aberdeen Proving Ground, MD, 1991.

3. Silling, S. A. "CTH Reference Manual: Boundary Layer Algorithm for Sliding in Two Dimensions." *SAND93-2487*, Sandia National Laboratories, Albuquerque, NM, 1994.

4. Silling, S. A. "Eulerian Simulation of the Perforation of Aluminum Plates by Nondeforming Projectiles." *SAND92-0493*, Sandia National Laboratories, Albuquerque, NM, 1992.

5. Kmetyk, L. N., and P. Yarrington. "CTH Analyses of Steel Rod Penetration Into Aluminum and Concrete Targets With Comparisons to Experimental Data." *SAND94-1498*, Sandia National Laboratories, Albuquerque, NM, 1994.

6. Magness Jr., L. S. Unpublished data. U.S. Army Research Laboratory, Aberdeen Proving Ground, MD, undated.

7. Scheffler, D. R. "CTH Hydrocode Predictions On the Effect of Rod Nose Shape On the Velocity at Which Tungsten Alloy Rods Transition From Rigid Body to Eroding Penetrators When Impacting Thick Aluminum Targets." *Structures Under Shock and Impact IV*, N. Jones, C. A. Brebbia, and A. J. Watson (eds.), pp. 297–310, *Proceedings of the Fourth International Conference On Structures Under Shock and Impact (SUSI96)*, Udine, Italy, July 3–6, 1996, Computational Mechanics Publications, Ashurst Lodge, Southampton, UK, 1996.

8. Johnson, G. R., and W. H. Cook. "A Constitutive Model and Data Subjected to Large Strains, High Strain Rates and High Temperatures." *Proceedings of the Seventh International Symposium on Ballistics*, pp. 541–547, The Hague, The Netherlands, 1983.

9. Zerilli, F. J., and R. W. Armstrong. "Dislocation-Mechanics-Based Constitutive Relations for Material Dynamics Calculations." *Journal of Applied Physics*, vol. 61, no. 5, pp. 1816–1825, 1987.

10. Steinberg, D. J., and C. M. Lund. "A Constitutive Model for Strain Rates From 10^{-4} to 10^{6} s^{-1}." *Journal of Applied Physics*, vol. 65, no. 4, pp. 1528–1533, 1989.

11. Steinberg, D. J., S. G. Cochran, and M. W. Guinan. "A Constitutive Model for Metal Applicable at High-Strain Rate." *Journal of Applied Physics*, vol. 51, no. 3, pp. 1498–1504, 1980.

12. Kerley, G. I. "CTH Equation of State Package: Porosity and Reactive Burn Models." *SAND92-0553*, Sandia National Laboratories, Albuquerque, NM, 1992.

13. Lee, E. L., H. C. Hornig, and J. W. Kury. "Adiabatic Expansion of High Explosive Detonation Products." *UCRL-50422*, Lawrence Livermore National Laboratory, Livermore, CA, 1968.

14. Johnson, G. R., and W. H. Cook. "Fracture Characteristics of Three Metals Subjected to Various Strains, Strain Rates, Temperatures, and Pressures." *Journal of Engineering Fracture Mechanics*, vol. 21, no. 1, pp. 31–48, 1985.

15. Noh, W. F., and P. Woodward. "SLIC (Simple Line Interface Calculation)." *Lecture Notes in Physics*, vol. 59, Springer-Verlag, Berlin, 1976.

16. Bell, R. L., and E. S. Hertel Jr. "An Improved Material Interface Reconstruction Algorithm for Eulerian Codes." *SAND92-1716*, Sandia National Laboratories, Albuquerque, NM, 1992.

17. Steinberg, D. J. "Equation of State and Strength Properties of Selected Materials." *UCRL-MA-106439*, Lawrence Livermore National Laboratory, Livermore, CA, 1991.

18. Forrestal, M. J., V. K. Luk, and N. S. Brar. "Perforation of Aluminum Armor Plates with Conical-Nose Projectiles." *Mechanics of Materials*, vol. 10, no. 1–2, pp. 97–105, 1990.

19. Boyer, H. E., and T. L. Gall (eds.). *Metals Handbook Desk Edition*, American Society for Metals, Metals Park, OH, 1985.

20. Bjerke, T. W., G. F. Silsby, D. R. Scheffler, and R. M. Mudd. "Yawed Long Rod Armor Penetration at Ordnance and Higher Velocities." *BRL-TR-3221*, U.S. Army Ballistic Research Laboratory, Aberdeen Proving Ground, MD, 1991.

21. Bjerke, T. W., G. F. Silsby, D. R. Scheffler, and R. M. Mudd. "Yawed Long-Rod Armor Penetration." *International Journal of Impact Engineering*, vol. 12, no. 2, pp. 281–292, 1992.

22. Forrestal, M. J., D. Y. Tzou, E. Askari, and D. B. Longscope. "Penetration Into Ductile Matel Targets With Rigid Spherical-Nose Rods." *International Journal of Impact Engineering*, vol. 16, no. 5–6, pp. 699–710, 1995.

23. Scheffler, D. R. "CTH Hydrocode Simulations of Hemisperical and Ogival Nose Tungsten Alloy Penetrators Perforating Finite Aluminum Targets." Y. S. Shin and J. A. Zukas (eds.), *Structures Under Extreme Loading Conditions*, PVP-vol. 325, pp. 125–136, ASME, New York, NY, 1996.

24. Magness Jr., L. S. Private communication. U.S. Army Research Laboratory, Aberdeen Proving Ground, MD, 1995.

25. Magness Jr., L. S. "Properties and Performance of KE Penetrator Materials." *Tungsten & Tungsten Alloys-1992,* A. Bose and R. J. Dowding (eds.), pp 15–22, *Proceedings of the First International Conference on Tungsten and Tungsten Alloys*, Arlington, Virginia, 1992, Metal Powder Industries Federation, Princeton, NJ, 1993.

26. Coates, R. S., and K. T. Ramesh. "The Deformation of Tungsten Alloys at High Strain Rates." *Shock-Wave and High-Strain-Rate Phenomena in Materials*, M. A. Meyers, L. E. Murr and K. P. Staudhammer (eds.), *Proceedings of the International Conference on the Material Effects of Shock-Wave and High-Strain-Rate Phenomena*, pp. 203–212, San Diego, CA, 1990, Marcel Dekker, Inc., New York, NY, 1992.

27. Zukas, J. A., T. Nicholas, L. B. Swift, and D. R. Curran. *Impact Dynamics*, Wiley-Interscience, New York, NY 1982.

INTENTIONALLY LEFT BLANK.

Appendix A:

CTH Input For Hemi-Nose Penetrator vs. 5083 Aluminum Target Using Pressure-Based Failure Model

INTENTIONALLY LEFT BLANK

```
* Run History
*
*eor* cgenin
*
nose shape tests: hemi v=1086 target=5083 al semi-infinite
*
control
 ep
 mmp
 viscosity bl=.1 bq=2 bs=0.1
endcontrol
*
mesh
 block 1 geom=2dc type=e
  x0 0.00
   x1 n 40    w 1.6891    rat 1.0
   x2 n 45  dxf 0.0422275  rat 1.05
  endx
  y0 -9.9390075
   y1 n 1545 dyf 0.0422275  rat 1.0
  endy
  xactive  0.0      0.4
  yactive -9.9390075 0.0
 endblock
endmesh
*
insertion
 block 1
  package '5083 Al target'
   material 1
   numsub 50
   insert box
    p1=0.0     0.0
    p2=7.6    53.34
   endinsert
  endpackage
  package 'w alloy rod nose'
   material 2
   numsub 100
*
*  NOTE: striking velocity (yvel) is changed below
*
    yvel 1.086e5
    insert circle
     ce=0.0    -0.33782
```

```
      r= 0.33782
     endinsert
    endpackage
    package 'w alloy rod body'
     material 2
     numsub 50
*
*  NOTE: striking velocity (yvel) is changed below
*
     yvel 1.086e5
     insert box
      p1=0.0     -0.33782
      p2=0.33782 -9.779
     endinsert
    endpackage
  endblock
endinsertion
*
epdata
 vpsave
*
*  NOTE: poisson ratio from for Tungsten from Metals Handbook, that for 5083 Aluminum
*        from  Forrestal, M.J., V. K. Luk, and N. S. Brar, "Perforation of aluminum with
*        conical-nose projectiles", Mechanic and Materials 10 (1990), pp. 97-105.
*
*  NOTE: properties for 5083 aluminum from Silling, S. A., "CTH Reference Manual: Boundary
*        Layer Algorithm for Sliding Interfaces in Two Dimensions", Sandia National
Laboratories
*        Report SAND93-2487, January 1994.
*
   matep 1
    johnson-cook='USER'  * NOTE: 5083-H131 ALUMINUM using undocumented power law
                ajo=-2.76e9  bjo=254.7    cjo=0.0
                mjo=1.0      njo=0.084    tjo=6.68e-2
                poisson 0.333
*
*  NOTE: actual tungsten alloy was 95W-2.5Ni-1.0Fe-1.5Co (21% swaged) with r0=18.1.
*        95W-3.5Ni-1.5Fe is being used to approximate the w alloy.
*
   matep 2
     steinberg='TUNGSTEN_NI_FE'
                r0st=18.16   tm0st=0.195002  atmst=1.3
                gm0st=1.67   ast=1.03e-12    bst=1.76396
                nst=0.13     c1st=0.0        c2st=0.0
                g0st=1.45e12 btst=7.7        eist=0.0
```

```
                ypst=0.0    ukst=0.0      ysmst=0.0
                yast=0.0    y0st=18.7e9   ymst=40.e9
                poisson=0.280
*
* NOTE: parameters for boundary layer algorithm taken similar to: Kmetyk, L. N. and P.
Yarrington,
*       "CTH Analysis of Steel Rod Penetration Into Aluminum and Concrete Targets with
*       Comparisons to Experimental Data", Sandia National Laboratories Report
SAND94-1498,
*       October 1994.
*
* NOTE: if BLINT model was not used in simulation the next line is commented out with "*"
*
  blint 1 soft 1 hard 2 wsl 0.084455 wbl 0.084455 fric=0.0 corr
  mix 3
endep
*
tracer
 block 1
 add 0. 0. to 0. -9.777 n 10
endtracer
*
edit
 block 1
  noexpanded
 endblock
endedit
*
eos
*
* NOTE: EOS properties from cth mgrun library
*
* NOTE: 5083-H131 Aluminum eos approximated with 6061-t6 Aluminum density reduced to
reflect
*       that for 5083 Aluminum from Metals Handbook Desk Edition.
*
 mat1 mgrun eos=6061-t6_al  r0=2.66   cs=0.534e6  s=1.4
                g0=1.97   cv=1.07e11
 mat2 mgrun eos=tungsten_ni r0=18.16  cs=0.403e6  s=1.237
                g0=1.67   cv=1.66e10
endeos
*
*eor* cthin
*
nose shape tests: hemi v=1086 target=5083 al semi-infinite
```

```
*
control
 tstop 600.e-6
 rdumpf 3600
 cpshift 999.
endcontrol
*
restart
*  file='rsct1'
 cycle=11049
endr
*
cellthermo
 mmp
 ntbad=99999
endc
*
convct
*
* NOTE: if KE Sim convection=0, if MV Sim convection=1
*
 convection=0
 interface=high_resolution
endconvct
*
edit
 shortt
  time 0. dtfrequency 150.e-6
 ends
 longt
  time 0. dtfrequency 600.e-6
 endl
 plott
  time 0. dtfrequency  50.e-6
 endp
 histt
  time 0. dtfrequency  0.3e-6
  htracer1
  htracer2
  htracer3
  htracer4
  htracer5
  htracer6
  htracer7
  htracer8
```

```
    htracer9
    htracer10
  endh
ende
*
boundary
  bhydro
    block 1
      bxbot 0
      bxtop 2
      bybot 2
      bytop 2
    endb
  endh
endb
*
fracts
  pressure
  pfrac1  -4.5e9
  pfrac2 -35.0e9
  pfmix   -1.0e20
  pfvoid  -1.0e20
endf
*
*eor* pltinp
*
```

INTENTIONALLY LEFT BLANK.

Appendix B:

CTH Input For Ogival-Nose Penetrator vs. 5083 Aluminum Target Using Pressure-Based Failure Model

INTENTIONALLY LEFT BLANK

```
* Run History
*
*eor* cgenin
*
nose shape tests: ogive v=923 target=5083 al semi-infinite
*
control
 ep
 mmp
 viscosity bl=.1 bq=2 bs=0.1
endcontrol
*
mesh
 block 1 geom=2dc type=e
  x0 0.00
   x1 n 40    w 1.6891    rat 1.0
   x2 n 45  dxf 0.0422275  rat 1.05
  endx
  y0 -10.219055
   y1 n 1545 dyf 0.0422275  rat 1.0
  endy
  xactive  0.0      0.4
  yactive -10.219055 0.0
 endblock
endmesh
*
insertion
 block 1
  package '5083 Al target'
   material 1
   numsub 50
   insert box
    p1=0.0     0.0
    p2=7.6    53.34
   endinsert
  endpackage
  package 'w alloy ogive nose rod'
   material 2
   numsub 100
*
*  NOTE: striking velocity (yvel) is changed below
*
   yvel 0.923e5
   insert uds
    point 0.0         0.0
```

```
      point 0.050437038 -0.08003015622
      point 0.095867718 -0.1600603124
      point 0.136665799 -0.2400904687
      point 0.173135779 -0.3201206249
      point 0.205527612 -0.4001507811
      point 0.234047376 -0.4801809373
      point 0.258865148 -0.5602110935
      point 0.280120900 -0.6402412498
      point 0.297928948 -0.7202714060
      point 0.312381319 -0.8003015622
      point 0.323550306 -0.8803317184
      point 0.331490355 -0.9603618746
      point 0.336239443 -1.040392031
      point 0.337820   -1.120422187
      point 0.337820  -10.1346
      point 0.0       -10.1346
      point 0.0        0.0
    endinsert
  endpackage
 endblock
endinsertion
*
epdata
 vpsave
*
* NOTE: poisson ratio from for Tungsten from Metals Handbook, that for 5083 Aluminum
*       from  Forrestal, M.J., V. K. Luk, and N. S. Brar, "Perforation of aluminum with
*       conical-nose projectiles", Mechanic and Materials 10 (1990), pp. 97-105.
*
* NOTE: properties for 5083 aluminum from Silling, S. A., "CTH Reference Manual: Boundary
*       Layer Algorithm for Sliding Interfaces in Two Dimensions", Sandia National Laboratories
*       Report SAND93-2487, January 1994.
*
  matep 1
   johnson-cook='USER'  * NOTE: 5083-H131 ALUMINUM using undocumented power law
               ajo=-2.76e9  bjo=254.7   cjo=0.0
               mjo=1.0     njo=0.084   tjo=6.68e-2
               poisson 0.333
*
* NOTE: actual tungsten alloy was 95W-2.5Ni-1.0Fe-1.5Co (21% swaged) with r0=18.1.
*       95W-3.5Ni-1.5Fe is being used to approximate the w alloy.
*
  matep 2
    steinberg='TUNGSTEN_NI_FE'
               r0st=18.16  tm0st=0.195002  atmst=1.3
```

```
                gm0st=1.67  ast=1.03e-12   bst=1.76396
                nst=0.13    c1st=0.0      c2st=0.0
                g0st=1.45e12 btst=7.7      eist=0.0
                ypst=0.0    ukst=0.0      ysmst=0.0
                yast=0.0    y0st=18.7e9   ymst=40.e9
                poisson=0.280
*
*  NOTE: parameters for boundary layer algorithm taken similar to: Kmetyk, L. N. and P. Yarrington,
*        "CTH Analysis of Steel Rod Penetration Into Aluminum and Concrete Targets with
*        Comparisons to Experimental Data", Sandia National Laboratories Report SAND94-1498,
*        October 1994.
*
* NOTE: if BLINT model was not used in simulation the next line is commented out with "*"
*
  blint 1 soft 1 hard 2 wsl 0.084455 wbl 0.084455 fric=0.0 corr
  mix 3
endep
*
tracer
 block 1
 add 0. 0. to 0. -10.1345 n 10
endtracer
*
edit
 block 1
  noexpanded
 endblock
endedit
*
eos
*
* eos properties from cth mgrun library
*
*  NOTE: EOS properties from cth mgrun library
*
*  NOTE: 5083-H131 Aluminum eos approximated with 6061-t6 Aluminum density reduced to reflect
*        that for 5083 Aluminum from Metals Handbook Desk Edition.
*
 mat1 mgrun eos=6061-t6_al  r0=2.66   cs=0.534e6  s=1.4
                  g0=1.97   cv=1.07e11
 mat2 mgrun eos=tungsten_ni r0=18.16  cs=0.403e6  s=1.237
                  g0=1.67   cv=1.66e10
endeos
```

```
*
*eor* cthin
*
nose shape tests: ogive v=923 target=5083 al semi-infinite
*
control
 tstop 600.e-6
 rdumpf 3600
 cpshift 999.
endcontrol
*
restart
*  file='rsct1'
 cycle=7465
endr
*
cellthermo
 mmp
 ntbad=99999
endc
*
convct
*
* NOTE: if KE Sim convection=0, if MV Sim convection=1
*
 convection=0
 interface=high_resolution
endconvct
*
edit
 shortt
  time 0. dtfrequency 150.e-6
 ends
 longt
  time 0. dtfrequency 600.e-6
 endl
 plott
  time 0. dtfrequency  50.e-6
 endp
 histt
  time 0. dtfrequency  0.3e-6
  htracer1
  htracer2
  htracer3
  htracer4
```

```
    htracer5
    htracer6
    htracer7
    htracer8
    htracer9
    htracer10
  endh
ende
*
boundary
  bhydro
    block 1
      bxbot 0
      bxtop 2
      bybot 2
      bytop 2
    endb
  endh
endb
*
fracts
  pressure
  pfrac1  -4.5e9
  pfrac2 -35.0e9
  pfmix   -1.0e20
  pfvoid  -1.0e20
endf
*
*eor* pltinp
```

INTENTIONALLY LEFT BLANK.

Appendix C:

CTH Input For Hemi-Nose Penetrator vs. 7039 Aluminum Target Using Pressure-Based Failure Model

INTENTIONALLY LEFT BLANK

```
* Run History
*
*eor* cgenin
*
nose shape tests: hemi v=1038 target=7039 al semi-infinite
*
control
 ep
 mmp
 viscosity bl=.1 bq=2 bs=0.1
endcontrol
*
mesh
 block 1 geom=2dc type=e
  x0 0.00
   x1 n 40    w 1.6891    rat 1.0
   x2 n 45   dxf 0.0422275  rat 1.05
  endx
  y0 -9.9390075
   y1 n 1545 dyf 0.0422275  rat 1.0
  endy
  xactive  0.0      0.4
  yactive -9.9390075 0.0
 endblock
endmesh
*
insertion
 block 1
  package '7039 Al target'
   material 1
   numsub 50
   insert box
    p1=0.0     0.0
    p2=7.6    53.34
   endinsert
  endpackage
*
  package 'w alloy rod nose'
   material 2
   numsub 100
*
* NOTE: striking velocity (yvel) is changed below
*
   yvel 1.038e5
   insert circle
```

```
      ce=0.0    -0.33782
      r= 0.33782
     endinsert
   endpackage
*
   package 'w alloy rod body'
    material 2
    numsub 50
*
*  NOTE: striking velocity (yvel) is changed below
*
    yvel 1.038e5
    insert box
     p1=0.0    -0.33782
     p2=0.33782 -9.779
    endinsert
   endpackage
 endblock
endinsertion
*
epdata
 vpsave
*
*  NOTE: poisson's ratio from Metals Handbook
*
   matep 1
    johnson-cook='7039_ALUMINUM'
                 ajo=3.3672e9 bjo=3.4293e9 cjo=0.01
                 mjo=1.0     njo=.41     tjo=7.76342e-2
                 poisson 0.345
*
*  NOTE: actual tungsten alloy was 95W-2.5Ni-1.0Fe-1.5Co (21% swaged) with r0=18.1.
*        95W-3.5Ni-1.5Fe is being used to approximate the w alloy.
*
   matep 2
     steinberg='TUNGSTEN_NI_FE'
                 r0st=18.16  tm0st=0.195002  atmst=1.3
                 gm0st=1.67  ast=1.03e-12   bst=1.76396
                 nst=0.13    c1st=0.0       c2st=0.0
                 g0st=1.45e12 btst=7.7       eist=0.0
                 ypst=0.0    ukst=0.0       ysmst=0.0
                 yast=0.0    y0st=18.7e9    ymst=40.e9
                 poisson=0.280
*
```

```
*  NOTE: parameters for boundary layer algorithm taken similar to: Kmetyk, L. N. and P. Yarrington,
*          "CTH Analysis of Steel Rod Penetration Into Aluminum and Concrete Targets with
*          Comparisons to Experimental Data", Sandia National Laboratories Report SAND94-1498,
*          October 1994.
*
*  NOTE: if BLINT model was not used in simulation the next line is commented out with "*"
*
   blint 1 soft 1 hard 2 wsl 0.084455 wbl 0.084455 fric=0.0 corr
   mix 3
endep
*
tracer
 block 1
 add 0. 0. to 0. -9.777 n 10
endtracer
*
edit
 block 1
  noexpanded
 endblock
endedit
*
eos
*
*  NOTE: EOS properties from cth mgrun library
*
*  NOTE: 7039 Aluminum eos approximated with 7075-t6 Aluminum. Density reduced to reflect that
*          for 7039 Aluminum from Johnson and Cook (1983).
*
 mat1 mgrun eos=7075-t6_al  r0=2.77   cs=0.520e6   s=1.36
                    g0=2.20   cv=1.07e11
 mat2 mgrun eos=tungsten_ni r0=18.16   cs=0.403e6   s=1.237
                    g0=1.67   cv=1.66e10
endeos
*
*eor* cthin
*
nose shape tests: hemi v=1038 target=7039 al semi-infinite
*
control
 tstop 600.e-6
 rdumpf 3600
 cpshift 999.
```

```
endcontrol
*
restart
*  file='rsct1'
  cycle=4727
endr
*
cellthermo
  mmp
  ntbad=99999
endc
*
convct
*
* NOTE: if KE Sim convection=0, if MV Sim convection=1
*
  convection=0
  interface=high_resolution
endconvct
*
edit
  shortt
    time 0. dtfrequency 150.e-6
  ends
  longt
    time 0. dtfrequency 600.e-6
  endl
  plott
    time 0. dtfrequency  50.e-6
  endp
  histt
    time 0. dtfrequency  0.3e-6
    htracer1
    htracer2
    htracer3
    htracer4
    htracer5
    htracer6
    htracer7
    htracer8
    htracer9
    htracer10
  endh
ende
*
```

```
boundary
 bhydro
  block 1
   bxbot 0
   bxtop 2
   bybot 2
   bytop 2
  endb
 endh
endb
*
fracts
 pressure
 pfrac1  -5.0e9
 pfrac2 -35.0e9
 pfmix   -1.0e20
 pfvoid  -1.0e20
endf
*
*eor* pltinp
```

INTENTIONALLY LEFT BLANK.

Appendix D:

CTH Input For Ogival-Nose Penetrator vs. 7039 Aluminum Target Using Pressure-Based Failure Model

INTENTIONALLY LEFT BLANK

```
* Run History
*
*eor* cgenin
*
nose shape tests: ogive v=1075 target=7039 al semi-infinite
*
control
 ep
 mmp
 viscosity bl=.1 bq=2 bs=0.1
endcontrol
*
mesh
 block 1 geom=2dc type=e
  x0 0.00
   x1 n 40    w 1.6891    rat 1.0
   x2 n 45  dxf 0.0422275  rat 1.05
  endx
  y0 -10.219055
   y1 n 1545 dyf 0.0422275  rat 1.0
  endy
  xactive  0.0      0.4
  yactive -10.219055 0.0
 endblock
endmesh
*
insertion
 block 1
  package '7039 Al target'
   material 1
   numsub 50
   insert box
    p1=0.0     0.0
    p2=7.6    53.34
   endinsert
  endpackage
*
  package 'w alloy ogive nose rod'
   material 2
   numsub 100
*
*  NOTE: striking velocity (yvel) is changed below
*
   yvel 1.075e5
   insert uds
```

```
      point 0.0         0.0
      point 0.050437038 -0.08003015622
      point 0.095867718 -0.1600603124
      point 0.136665799 -0.2400904687
      point 0.173135779 -0.3201206249
      point 0.205527612 -0.4001507811
      point 0.234047376 -0.4801809373
      point 0.258865148 -0.5602110935
      point 0.280120900 -0.6402412498
      point 0.297928948 -0.7202714060
      point 0.312381319 -0.8003015622
      point 0.323550306 -0.8803317184
      point 0.331490355 -0.9603618746
      point 0.336239443 -1.040392031
      point 0.337820    -1.120422187
      point 0.337820   -10.1346
      point 0.0       -10.1346
      point 0.0         0.0
    endinsert
  endpackage
 endblock
endinsertion
*
epdata
 vpsave
  matep 1
   johnson-cook='7039_ALUMINUM'
                ajo=3.3672e9 bjo=3.4293e9 cjo=0.01
                mjo=1.0     njo=.41     tjo=7.76342e-2
                poisson 0.345
*
* NOTE: actual tungsten alloy was 95W-2.5Ni-1.0Fe-1.5Co (21% swaged) with r0=18.1.
*         95W-3.5Ni-1.5Fe is being used to approximate the w alloy.
*
  matep 2
    steinberg='TUNGSTEN_NI_FE'
                r0st=18.16   tm0st=0.195002  atmst=1.3
                gm0st=1.67   ast=1.03e-12    bst=1.76396
                nst=0.13     c1st=0.0        c2st=0.0
                g0st=1.45e12 btst=7.7        eist=0.0
                ypst=0.0     ukst=0.0        ysmst=0.0
                yast=0.0     y0st=18.7e9     ymst=40.e9
                poisson=0.280
*
```

```
*  NOTE: parameters for boundary layer algorithm taken similar to: Kmetyk, L. N. and P. Yarrington,
*          "CTH Analysis of Steel Rod Penetration Into Aluminum and Concrete Targets with
*          Comparisons to Experimental Data", Sandia National Laboratories Report SAND94-1498,
*          October 1994.
*
* NOTE: if BLINT model was not used in simulation the next line is commented out with "*"
*
   blint 1 soft 1 hard 2 wsl 0.084455 wbl 0.084455 fric=0.0 corr
   mix 3
endep
*
tracer
 block 1
 add 0. 0. to 0. -10.1345 n 10
endtracer
*
edit
 block 1
  noexpanded
 endblock
endedit
*
eos
*
* NOTE: EOS properties from cth mgrun library
*
* NOTE: 7039 Aluminum eos approximated with 7075-t6 Aluminum. Density reduced to reflect that
*          for 7039 Aluminum from Johnson and Cook (1983).
*
 mat1 mgrun eos=7075-t6_al  r0=2.77   cs=0.520e6   s=1.36
                    g0=2.20   cv=1.07e11
 mat2 mgrun eos=tungsten_ni r0=18.16  cs=0.403e6   s=1.237
                    g0=1.67   cv=1.66e10
endeos
*
*eor* cthin
*
nose shape tests: ogive v=1075 target=7039 al semi-infinite
*
control
 tstop 600.e-6
 rdumpf 3600
 cpshift 999.
```

```
endcontrol
*
restart
*  file='rsct1'
  cycle=4691
endr
*
cellthermo
  mmp
  ntbad=99999
endc
*
convct
*
* NOTE: if KE Sim convection=0, if MV Sim convection=1
*
  convection=0
  interface=high_resolution
endconvct
*
edit
  shortt
    time 0. dtfrequency 150.e-6
  ends
  longt
    time 0. dtfrequency 600.e-6
  endl
  plott
    time 0. dtfrequency  50.e-6
  endp
  histt
    time 0. dtfrequency  0.3e-6
    htracer1
    htracer2
    htracer3
    htracer4
    htracer5
    htracer6
    htracer7
    htracer8
    htracer9
    htracer10
  endh
ende
*
```

```
boundary
 bhydro
  block 1
   bxbot 0
   bxtop 2
   bybot 2
   bytop 2
  endb
 endh
endb
*
fracts
 pressure
 pfrac1  -5.0e9
 pfrac2 -35.0e9
 pfmix   -1.0e20
 pfvoid  -1.0e20
endf
*
*eor* pltinp
```

INTENTIONALLY LEFT BLANK.

Appendix E:

CTH Input For Hemi-Nose Penetrator vs. 5083 Aluminum Target Using Strain-Based Failure Model

INTENTIONALLY LEFT BLANK

```
* Run History
*
*eor* cgenin
*
nose shape tests: hemi v=1296 target=5083 al semi-infinite
*
control
 ep
 mmp
 viscosity bl=.1 bq=2 bs=0.1
endcontrol
*
mesh
 block 1 geom=2dc type=e
  x0 0.00
   x1 n 40    w 1.6891    rat 1.0
   x2 n 45   dxf 0.0422275  rat 1.05
  endx
  y0 -9.9390075
   y1 n 1545 dyf 0.0422275  rat 1.0
  endy
  xactive  0.0      0.4
  yactive -9.9390075 0.0
 endblock
endmesh
*
insertion
 block 1
  package '5083 Al target'
   material 1
   numsub 50
   insert box
    p1=0.0     0.0
    p2=7.6    53.34
   endinsert
  endpackage
*
  package 'w alloy rod nose'
   material 2
   numsub 100
*
* NOTE: striking velocity (yvel) is changed below
*
   yvel 1.296e5
   insert circle
```

```
      ce=0.0    -0.33782
      r= 0.33782
     endinsert
   endpackage
*
   package 'w alloy rod body'
    material 2
    numsub 50
*
*  NOTE: striking velocity (yvel) is changed below
*
    yvel 1.296e5
    insert box
     p1=0.0    -0.33782
     p2=0.33782 -9.779
    endinsert
   endpackage
 endblock
endinsertion
*
epdata
 vpsave
*
*  NOTE: poisson ratio from for Tungsten from Metals Handbook, that for 5083 Aluminum
*        from  Forrestal, M.J., V. K. Luk, and N. S. Brar, "Perforation of aluminum with
*        conical-nose projectiles", Mechanic and Materials 10 (1990), pp. 97-105.
*
*  NOTE: properties for 5083 aluminum from Silling, S. A., "CTH Reference Manual: Boundary
*        Layer Algorithm for Sliding Interfaces in Two Dimensions", Sandia National Laboratories
*        Report SAND93-2487, January 1994.
*
   matep 1
    johnson-cook='USER'  * NOTE: 5083-H131 ALUMINUM using undocumented power law
                ajo=-2.76e9  bjo=254.7    cjo=0.0
                mjo=1.0      njo=0.084    tjo=6.68e-2
                poisson 0.333
*
*  NOTE: for strain failure at 150% on parameter for Johnson-Cook fracture model except the first
*        are set to zero.
*
        jfrac='USER' jfd1=1.5 jfd2=0.0 jfd3=0.0 jfd4=0.0 jfd5=0.0
                jftm=0.0 jfpf0=-4.5e9
*
*  NOTE: actual tungsten alloy was 95W-2.5Ni-1.0Fe-1.5Co (21% swaged) with r0=18.1.
*        95W-3.5Ni-1.5Fe is being used to approximate the w alloy.
```

```
*
  matep 2
    steinberg='TUNGSTEN_NI_FE'
              r0st=18.16  tm0st=0.195002  atmst=1.3
              gm0st=1.67  ast=1.03e-12  bst=1.76396
              nst=0.13  c1st=0.0  c2st=0.0
              g0st=1.45e12 btst=7.7  eist=0.0
              ypst=0.0  ukst=0.0  ysmst=0.0
              yast=0.0  y0st=18.7e9  ymst=40.e9
              poisson=0.280
*
* NOTE: for strain failure at 150% on parameter for Johnson-Cook fracture model except the first
*       are set to zero.
*
      jfrac='USER' jfd1=1.5 jfd2=0.0 jfd3=0.0 jfd4=0.0 jfd5=0.0
              jftm=0.0 jfpf0=-35.e9
*
*  NOTE: parameters for boundary layer algorithm taken similar to: Kmetyk, L. N. and P. Yarrington,
*       "CTH Analysis of Steel Rod Penetration Into Aluminum and Concrete Targets with
*       Comparisons to Experimental Data", Sandia National Laboratories Report SAND94-1498,
*       October 1994.
*
* NOTE: if BLINT model was not used in simulation the next line is commented out with "*"
*
  blint 1 soft 1 hard 2 wsl 0.084455 wbl 0.084455 fric=0.0 corr
  mix 3
endep
*
tracer
 block 1
 add 0. 0. to 0. -9.777 n 10
endtracer
*
edit
 block 1
  noexpanded
 endblock
endedit
*
eos
*
* eos properties from cth mgrun library
*
* 5083-H131 Aluminum eos approximated with 6061-t6 Aluminum
```

```
* density reduced to reflect that for 5083 Aluminum from
* Metal's Handbook.
 mat1 mgrun eos=6061-t6_al  r0=2.66   cs=0.534e6  s=1.4
                    g0=1.97   cv=1.07e11
 mat2 mgrun eos=tungsten_ni r0=18.16  cs=0.403e6  s=1.237
                    g0=1.67   cv=1.66e10
endeos
*
*eor* cthin
*
nose shape tests: hemi v=1296 target=5083 al semi-infinite
*
control
 tstop 600.e-6
 rdumpf 3600
 cpshift 999.
endcontrol
*
restart
*  file='rsct1'
 cycle=15972
endr
*
cellthermo
 mmp
 ntbad=99999
endc
*
convct
*
* NOTE: if KE Sim convection=0, if MV Sim convection=1
*
 convection=0
 interface=high_resolution
endconvct
*
edit
 shortt
  time 0. dtfrequency 150.e-6
 ends
 longt
  time 0. dtfrequency 600.e-6
 endl
 plott
  time 0. dtfrequency  50.e-6
```

```
 endp
 histt
  time 0. dtfrequency  0.3e-6
  htracer1
  htracer2
  htracer3
  htracer4
  htracer5
  htracer6
  htracer7
  htracer8
  htracer9
  htracer10
 endh
ende
*
boundary
 bhydro
  block 1
   bxbot 0
   bxtop 2
   bybot 2
   bytop 2
  endb
 endh
endb
*
fracts
 pressure
 pfrac1  -4.5e9
 pfrac2 -35.0e9
 pfmix   -1.0e20
 pfvoid  -1.0e20
endf
*
*eor* pltinp
*
units=cgsk
allcells=off
color void 0
color table 4
color void 0
```

INTENTIONALLY LEFT BLANK

NO. OF COPIES	ORGANIZATION
2	DEFENSE TECHNICAL INFORMATION CENTER DTIC DDA 8725 JOHN J KINGMAN RD STE 0944 FT BELVOIR VA 22060-6218
1	HQDA DAMO FDQ DENNIS SCHMIDT 400 ARMY PENTAGON WASHINGTON DC 20310-0460
1	CECOM SP & TRRSTRL COMMCTN DIV AMSEL RD ST MC M H SOICHER FT MONMOUTH NJ 07703-5203
1	PRIN DPTY FOR TCHNLGY HQ US ARMY MATCOM AMCDCG T M FISETTE 5001 EISENHOWER AVE ALEXANDRIA VA 22333-0001
1	PRIN DPTY FOR ACQUSTN HQS US ARMY MATCOM AMCDCG A D ADAMS 5001 EISENHOWER AVE ALEXANDRIA VA 22333-0001
1	DPTY CG FOR RDE HQS US ARMY MATCOM AMCRD BG BEAUCHAMP 5001 EISENHOWER AVE ALEXANDRIA VA 22333-0001
1	ASST DPTY CG FOR RDE HQS US ARMY MATCOM AMCRD COL S MANESS 5001 EISENHOWER AVE ALEXANDRIA VA 22333-0001

NO. OF COPIES	ORGANIZATION
1	DPTY ASSIST SCY FOR R&T SARD TT F MILTON THE PENTAGON RM 3E479 WASHINGTON DC 20310-0103
1	DPTY ASSIST SCY FOR R&T SARD TT D CHAIT THE PENTAGON WASHINGTON DC 20310-0103
1	DPTY ASSIST SCY FOR R&T SARD TT K KOMINOS THE PENTAGON WASHINGTON DC 20310-0103
1	DPTY ASSIST SCY FOR R&T SARD TT B REISMAN THE PENTAGON WASHINGTON DC 20310-0103
1	DPTY ASSIST SCY FOR R&T SARD TT T KILLION THE PENTAGON WASHINGTON DC 20310-0103
1	OSD OUSD(A&T)/ODDDR&E(R) J LUPO THE PENTAGON WASHINGTON DC 20301-7100
1	INST FOR ADVNCD TCHNLGY THE UNIV OF TEXAS AT AUSTIN PO BOX 202797 AUSTIN TX 78720-2797
1	DUSD SPACE 1E765 J G MCNEFF 3900 DEFENSE PENTAGON WASHINGTON DC 20301-3900
1	USAASA MOAS AI W PARRON 9325 GUNSTON RD STE N319 FT BELVOIR VA 22060-5582

NO. OF
COPIES ORGANIZATION

1 CECOM
PM GPS COL S YOUNG
FT MONMOUTH NJ 07703

1 GPS JOINT PROG OFC DIR
COL J CLAY
2435 VELA WAY STE 1613
LOS ANGELES AFB CA 90245-5500

1 ELECTRONIC SYS DIV DIR
CECOM RDEC
J NIEMELA
FT MONMOUTH NJ 07703

3 DARPA
L STOTTS
J PENNELLA
B KASPAR
3701 N FAIRFAX DR
ARLINGTON VA 22203-1714

1 SPCL ASST TO WING CMNDR
50SW/CCX
CAPT P H BERNSTEIN
300 O'MALLEY AVE STE 20
FALCON AFB CO 80912-3020

1 USAF SMC/CED
DMA/JPO
M ISON
2435 VELA WAY STE 1613
LOS ANGELES AFB CA 90245-5500

1 US MILITARY ACADEMY
MATH SCI CTR OF EXCELLENCE
DEPT OF MATHEMATICAL SCI
MDN A MAJ DON ENGEN
THAYER HALL
WEST POINT NY 10996-1786

1 DIRECTOR
US ARMY RESEARCH LAB
AMSRL CS AL TP
2800 POWDER MILL RD
ADELPHI MD 20783-1145

NO. OF
COPIES ORGANIZATION

1 DIRECTOR
US ARMY RESEARCH LAB
AMSRL CS AL TA
2800 POWDER MILL RD
ADELPHI MD 20783-1145

3 DIRECTOR
US ARMY RESEARCH LAB
AMSRL CI LL
2800 POWDER MILL RD
ADELPHI MD 20783-1145

ABERDEEN PROVING GROUND

2 DIR USARL
AMSRL CI LP (305)

NO. OF COPIES	ORGANIZATION
6	CDR US ARMY ARDEC AMSTA AR AEE WW E BAKER C CHIN R FONG J PEARSON J WALSH TECH LIB PICATINNY ARSNL NJ 07806-5000
1	CDR US ARMY ARDEC AMSTA AR AET M TECH LIB PICATINNY ARSNL NJ 07806-5000
1	CDR US ARMY ARDEC AMSTA AR FS E ANDRICOPOULOS PICATINNY ARSNL NJ 07806-5000
3	CDR US ARMY MERDEC AMSME RD ST WF L CRAFT D LOVELACE M SCHEXNAYDER REDSTONE ARSNL AL 35898-5250
1	DIR US ARO WASH AMXRO W K A BANNISTER RM 8N31 5001 EISENHOWER AVE ALEXANDRIA VA 22333-0001
3	DIR US ARO J CHANDRA K IYER TECH LIB PO BOX 12211 RSCH TRIANGLE PK NC 27709-2211
4	CDR US ARMY COE J BALSARA T BLEVINS P PAPIDOS R NAMBURA 3909 HALL FERRY RD VICKSBURG MS 39180-6199

NO. OF COPIES	ORGANIZATION
3	DIR US ARMY DARPA J RICHARDSON TECH INFO B WILCOX 3701 N FAIRFAX DR ARLINGTON VA 22203-1714
2	CDR US ARMY TACOM AMSTA RSK J THOMPSON S GOODMAN WARREN MI 48397-5000
2	DIR NRL J A NEMES A E WILLIAMS CODE 6684 4555 OVERLOOK AVE SW WASH DC 20375
2	CDR NSWC W H HOLT CODE G22 W MOCK 17320 DAHLGREN RD DAHLGREN VA 22448-5000
8	CDR NSWC C S COFFEY R K GARRETT JR H MAIR R12 J MCKIRGAN B PARK D G TASKER TECH LIB F ZERILLI 10901 NEW HAMPSHIRE AVE SILVER SPRING MD 20903-5000
2	CDR NWC T GILL CODE 3261 TECH LIB CHINA LAKE CA 93555-6001
1	NAVAL POST GRAD SCHL J STERNBERG CODE 73 MONTEREY CA 93943

NO. OF COPIES	ORGANIZATION
1	USAF PHILLIPS LAB PL WSCD F ALLAHDADI KIRKLAND AFB NM 87185
1	USAF WAL T NICHOLAS WRIGHT PAT AFB OH 45433
4	USAF WL MNMW W COOK J FOSTER M NIXON TECH LIB EGLIN AFB FL 32542-5434
14	DIR LANL T F ADAMS F663 J BOLSTAD G787 J CHAKYAK R DAVIDSON K557 E FERM P FOLLANSBEE F663 G T GRAY III B295 K HOLIAN B295 L HULL J JOHNSON F663 D A MANDELL F663 P MAULIN L SCHWALBE TECH LIB PO BOX 1663 LOS ALAMOS NM 87454
12	DIR LLNL B R BOWMAN L122 R COUCH L35 M FINGER L38 W H GOURDIN G GOUDREAU C HOOVER D LASSILA L342 P RABOIN J E REAUGH L290 M J MURPHY TECH LIB R E TIPTON L35 PO BOX 1663 LOS ALAMOS NM 87545

NO. OF COPIES	ORGANIZATION
2	DIR SNL D BAMMANN M CHIESA LIVERMORE CA 94550
9	DIR SNL R M BRANNON DIV 1432 L C CHHABILDAS MS 0821 M FORRESTAL DIV 1551 E S HERTEL JR MS 0819 M KIPP DIV 1533 J M MCGLAUN MS 0819 S A SILLING T TRUCANO MS 0819 P YARRINGTON DIV 1533 PO BOX 5800 ALBUQUERQUE NM 87185-0307
5	IAT UNIV OF TX AUSTIN S J BLESS H D FAIR T M KIEHNE M J NORMANDIA D LITTLEFIELD 4030 2 W BRAKER LN AUSTIN TX 78759-5329
3	SOUTHWEST RSCH INST C ANDERSON S MULLIN J WALKER 8500 CULEBRA RD PO DRAWER 28510 SAN ANTONIO TX 78284
1	AEROJET ELECTRO SYS CO WARHEAD SYSTEMS J CARLEONE PO BOX 296 AZUSA CA 91702
4	ALLIANT TECHSYS INC S BEISSEL T HOLMQUIST MN11 2720 R STRYK G R JOHNSON MN11 2925 7225 NORTHLAND DR BROOKLYN PK MN 55428

NO. OF COPIES	ORGANIZATION
1	ALME AND ASSOC M L ALME 102 STEVENS FOREST PROF 9650 SANTIAGO RD COLUMBIA MD 21045
1	APPLIED RSCH ASSOC INC J D YATTEAU 5941 S MIDDLEFIELD RD STE 100 LITTLETON CO 80123
2	APPLIED RSCH ASSOC INC T C CARNEY F MAESTAS 4300 SAN MATEO BLVD SE STE A220 ALBUQUERQUE NM 87110
1	BRIGS CO J E BACKOFEN 2668 PETERSBOUGH ST HERNDON VA 22071-2443
3	DYNA EAST CORP P C CHOU R CICCARELLI W FLIS 3620 HORIZON DRIVE KING OF PRUSSIA PA 19406
2	GEN RSCH CORP ATTN A CHARTERS T MENNA 5383 HOLLISTER AVE SANTA BARBARA CA 93111
1	IRA INC D ORPHAL 4450 BLACK AVE STE E PLEASANTON CA 94566
1	KAMAN SCIENCES CORP J S WILBECK 7600 BLVD S STE 208 HUNTSVILLE AL 35802
1	KAMAN SCIENCES CORP N ARI PO BOX 7463 COLORADO STRINGS CO 80933-7463
1	D R KENNEDY & ASSOC INC D KENNEDY PO BOX 4003 MOUNTAIN VIEW CA 94040
1	KERLEY PUB SVC G I KERLEY PO BOX 13835 ALBUQUERQUE NM 87192-3835
3	LIVERMORE SOFTWARE TECH CORP J O HALLQUIST B MAKER D STILLMAN 2876 WAVERLY WAY LIVERMORE CA 94550
1	ORLANDO TECH INC D A MATUSKA PO BOX 855 SHALIMAR FL 32579
2	SRI INTERNATIONAL D CURRAN L SEAMAN 333 RAVENSWOOD AVE MENLO PARK CA 94025
1	ZERNOW TECH SVC INC L ZERNOW 425 W BONITA AVE STE 208 SAN DIMAS CA 91773
1	COMPUTATIONAL MECH ASSOC J A ZUKAS PO BOX 11314 BALTIMORE MD 21239-0314
1	S CUBED R SEDGWICK PO BOX 1620 LA JOLLA CA 92038-1620

NO. OF
COPIES ORGANIZATION

ABERDEEN PROVING GROUND

1 DIR AMSAA
R THOMPSON

56 DIR USARL
AMSRL SL B, P DIETZ (328)
AMSRL SL BC, J T KOLPCIC (328)
AMSRL SL BV,
R SAUCIER (247)
R SHNIDMAN (247)
J R STROBEL (247)
AMSRL WM, D ECCLESHALL
AMSRL WM MA S, J BEATTY
S CHOU
J DANDEKAR
D J GROVE
A RAJENDRAN
T WEERASOORIYA
AMSRL WM PD,
G GAZONAS
D HOPKINS
S WILKERSON
AMSRL WM T, W MORRISON
AMSRL WM TA,
W BRUCHEY JR
G FILBEY JR
W GILLICH
W GOOCH JR
Y HAUNG
H MEYER JR
J DEHN
S BILYK
E RAPACKI JR
G BULMASH
AMSRL WM TB,
R FREY
J STARKENBERG
R LOTTERO
AMSRL WM TC,
T BJERKE
R COATES
W S DE ROSSET
F GRACE
K KIMSEY
M LAMPSON
T SHERRICK
S SCHRAML
L MAGNESS

NO. OF
COPIES ORGANIZATION

W WALTERS
D SCHEFFLER (4 CP)
AMSRL WM TD,
R L BITTING
A M DIETRICH JR
T FARRAND
K FRANK
N GNIAZDOWSKI
F GREGORY
P KINGMAN
M RAFTENBERG
G RANDERS-PEHRSON
M SCHEIDLER
S SCHOENFELD
S SEGLETES
J WALTER JR
T W WRIGHT

REPORT DOCUMENTATION PAGE

Form Approved
OMB No. 0704-0188

1. AGENCY USE ONLY *(Leave blank)*	2. REPORT DATE	3. REPORT TYPE AND DATES COVERED
	July 1997	Final, Jul 95 - Feb 97

4. TITLE AND SUBTITLE
Modeling the Effect of Penetrator Nose Shape on Threshold Velocity for Thick Aluminum Targets

5. FUNDING NUMBERS
PR: 1L162618AH80

6. AUTHOR(S)
Daniel R. Scheffler

7. PERFORMING ORGANIZATION NAME(S) AND ADDRESS(ES)
U.S. Army Research Laboratory
ATTN: AMSRL-WM-TC
Aberdeen Proving Ground, MD 21005-5066

8. PERFORMING ORGANIZATION REPORT NUMBER
ARL-TR-1417

9. SPONSORING/MONITORING AGENCY NAMES(S) AND ADDRESS(ES)

10.SPONSORING/MONITORING AGENCY REPORT NUMBER

11. SUPPLEMENTARY NOTES

12a. DISTRIBUTION/AVAILABILITY STATEMENT
Approved for public release; distribution is unlimited.

12b. DISTRIBUTION CODE

13. ABSTRACT *(Maximum 200 words)*

This study examines the ability of the CTH hydrocode to predict the effects of rod nose shape on the threshold impact velocity, whereby tungsten alloy long rods transition from rigid-body to eroding-rod penetration during penetration or perforation of thick aluminum targets. Two rod nose shapes (hemispherical and ogival) were used in the simulations, and two aluminum alloys (5083 and 7039) were used as the target materials. The predicted results are compared to an experimental study. Predictions of the threshold velocity for the ogival-nose rod are offered.

14. SUBJECT TERMS
penetrator, impact, hydrocode, penetration, rigid body penetrator, tungsten, aluminum, threshold velocity

15. NUMBER OF PAGES
59

16. PRICE CODE

17. SECURITY CLASSIFICATION OF REPORT	18. SECURITY CLASSIFICATION OF THIS PAGE	19. SECURITY CLASSIFICATION OF ABSTRACT	20. LIMITATION OF ABSTRACT
UNCLASSIFIED	UNCLASSIFIED	UNCLASSIFIED	UL

NSN 7540-01-280-5500

Standard Form 298 (Rev. 2-89)
Prescribed by ANSI Std. 239-18 298-102

INTENTIONALLY LEFT BLANK.

USER EVALUATION SHEET/CHANGE OF ADDRESS

This Laboratory undertakes a continuing effort to improve the quality of the reports it publishes. Your comments/answers to the items/questions below will aid us in our efforts.

1. ARL Report Number/Author ARL-TR-1417 (Scheffler) Date of Report July 1997

2. Date Report Received _____

3. Does this report satisfy a need? (Comment on purpose, related project, or other area of interest for which the report will be used.) _____

4. Specifically, how is the report being used? (Information source, design data, procedure, source of ideas, etc.) _____

5. Has the information in this report led to any quantitative savings as far as man-hours or dollars saved, operating costs avoided, or efficiencies achieved, etc? If so, please elaborate. _____

6. General Comments. What do you think should be changed to improve future reports? (Indicate changes to organization, technical content, format, etc.) _____

CURRENT ADDRESS

_____
Organization

_____
Name E-mail Name

_____
Street or P.O. Box No.

_____
City, State, Zip Code

7. If indicating a Change of Address or Address Correction, please provide the Current or Correct address above and the Old or Incorrect address below.

OLD ADDRESS

_____
Organization

_____
Name

_____
Street or P.O. Box No.

_____
City, State, Zip Code

(Remove this sheet, fold as indicated, tape closed, and mail.)
(DO NOT STAPLE)

DEPARTMENT OF THE ARMY

OFFICIAL BUSINESS

NO POSTAGE
NECESSARY
IF MAILED
IN THE
UNITED STATES

BUSINESS REPLY MAIL
FIRST CLASS PERMIT NO 0001,APG,MD

POSTAGE WILL BE PAID BY ADDRESSEE

DIRECTOR
US ARMY RESEARCH LABORATORY
ATTN AMSRL WM TC
ABERDEEN PROVING GROUND MD 21005-5066